Eur. Phys. J. C 12, 25–33 (2000)
Digital Object Identifier (DOI) 10.1007/s100529900222

THE EUROPEAN PHYSICAL JOURNAL C


# Experimental study of the processes $e^+e^- \to \phi \to \eta\gamma, \pi^0\gamma$ at VEPP-2M*

M.N. Achasov, A.V. Berdyugin, A.V. Bozhenok, D.A. Bukin, S.V. Burdin, T.V. Dimova, V.P. Druzhinin, M.S. Dubrovin, I.A. Gaponenko, V.B. Golubev, V.N. Ivanchenko, A.A. Korol, S.V. Koshuba, E.V. Pakhtusova, A.A. Salnikov[a], S.I. Serednyakov, V.V. Shary, Yu.M. Shatunov, V.A. Sidorov, Z.K. Silagadze

Budker Institute of Nuclear Physics, 630090 Novosibirsk, Russia

Received: 26 April 1999 / Revised version: 18 June 1999 / Published online: 16 November 1999

**Abstract.** The processes $e^+e^- \to \eta\gamma, \pi^0\gamma \to 3\gamma$ were studied in the SND experiment at the VEPP-2M collider in the energy region of the $\phi$ meson. The branching ratios obtained in this study are $\mathrm{Br}(\phi \to \eta\gamma) = (1.338 \pm 0.012 \pm 0.052)\%$ and $\mathrm{Br}(\phi \to \pi^0\gamma) = (1.226 \pm 0.036^{+0.096}_{-0.089}) \times 10^{-3}$. A comparison of the experimental data with different theoretical models was performed.

## 1 Introduction

Studies of the radiative decays of the light vector mesons $(\rho, \omega, \phi)$ in $e^+e^-$ collisions play an important role in understanding of the electromagnetic structure of $q\bar{q}$ states and of the low-energy behavior of the strong interactions [1]. Theoretical models employed here describe radiative decays of the mesons [2–4] and the hadronization processes in $e^+e^-$ collisions [5,6]. Unfortunately, the statistics collected on $e^+e^-$ colliders in the low-energy region presently does not allow one to make an unambiguous determination of the parameters of these models or to distinguish between the different models. With the beginning of the CMD-2 [7] and SND [8] experiments at the VEPP-2M collider, a new opportunity emerges to significantly increase the experimental statistics and reduce the uncertainties of the observed results.

In this work we present the results of studies of the processes $e^+e^- \to \eta\gamma, \pi^0\gamma$ in the three-photon final state in the $\phi$ meson region, which were obtained with the experimental data gathered in the SND experiment. Previous information on these processes is mainly from the ND [9], CMD-2 [10], and SND [11] measurements. Sect. 2 gives a brief description of the apparatus and the experimental conditions, Sect. 3 describes the data analysis procedure, Sect. 4 gives the results obtained for the different theoretical models, and Sect. 5 briefly discusses the results obtained.

* This work is partially supported by RFBR (grant Nos. 96-02-19192 and 96-15-96327) and STP "Integration" (grant No. 274).

[a] Corresponding author, e-mail: salnikov@inp.nsk.su

## 2 Apparatus and experimental conditions

SND is a general-purpose non-magnetic detector (Fig. 1). A more detailed description of the detector can be found in [8]. SND was designed and optimized for the observation of neutral particles. The main part of the detector is an electromagnetic calorimeter build of 1632 NaI(Tl) crystals. The full thickness of the calorimeter for the particles originating from the interaction point is $13.5X_0$. The calorimeter provides a good energy resolution for photons (Fig. 2), which can be approximated as $\sigma_E(E)/E = 4.2\%/E(\mathrm{GeV})^{1/4}$ [12]. The angular resolution is determined primarily by the size of the crystals and is approximately equal to $\sigma_{\theta,\varphi} = 1.5^\circ$ [13]. The calorimeter and the event reconstruction program allow one to detect photons with the energies above 20 MeV with a solid angle coverage 90% of $4\pi$.

The experiments with the SND detector were carried out at the VEPP-2M collider with the average luminosity of $\sim 10^{30}\,\mathrm{cm}^{-2}\mathrm{s}^{-1}$. In this work we present the results based on the experimental statistics collected during 1996 year, which includes 7 scans of the energy region 985–1040 MeV. The total integrated luminosity accumulated in these scans is $4.3\,\mathrm{pb}^{-1}$, corresponding to approximately $8.2 \times 10^6$ events of $\phi$ meson decays.

## 3 Data analysis

In this work two radiative decays of $\phi$ meson were studied, namely in the following processes:

$$e^+e^- \to \eta\gamma \to \gamma\gamma\gamma, \tag{1}$$

$$e^+e^- \to \pi^0\gamma \to \gamma\gamma\gamma, \tag{2}$$

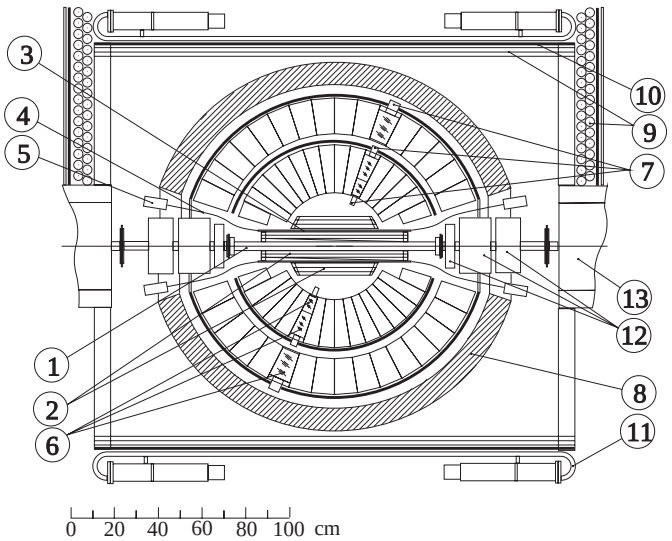


**Fig. 1.** SND detector, cut along the beams; 1 beam pipe, 2 drift chambers, 3 scintillation counters, 4 light guides, 5 PMTs, 6 NaI(Tl) crystals, 7 vacuum phototriodes, 8 iron absorber, 9 streamer tubes, 10 1 cm iron plates, 11 scintillation counters, 12 and 13 elements of the collider magnetic system

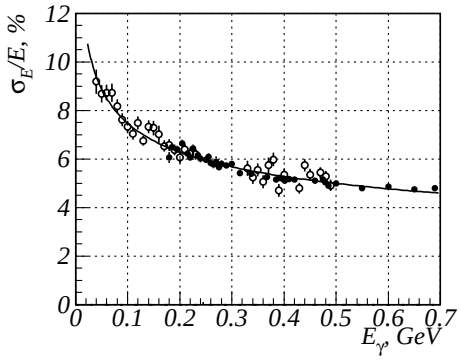


**Fig. 2.** Energy dependence of the calorimeter energy resolution. The data were obtained from $e^+e^- \to \gamma\gamma$ (dots) and $e^+e^- \to e^+e^-\gamma$ (open circles) processes

with the main background coming from non-resonant QED three-quanta annihilation:

$$e^+e^- \to \gamma\gamma\gamma(\text{QED}). \tag{3}$$

For studies of the cross sections of the investigated processes near the resonance maximum a procedure was developed for the selection of events with three detected photons. For the suppression of spurious signals in the calorimeter, which appear mainly in the crystals closest to the beam, additional restrictions were imposed on the energies and angles of the reconstructed photons. These restrictions were based on a detailed study of $e^+e^- \to \gamma\gamma$ events. The preliminary selection included the following conditions:

(1) the presence of three or four reconstructed photons,
(2) the total energy deposition in the calorimeter ($E_{\text{tot}}$) is in the range from $0.7s^{1/2}$ to $1.2s^{1/2}$, where $s = 4E^2_{\text{beam}}$,
(3) the sum of the momenta of all particles is lower than $0.2E_{\text{tot}}/c$,
(4) the minimal energy of the photons is 50 MeV; the polar angle for the photons with energies 50–100 MeV is in the range $45° < \theta < 135°$, for the photons with the energies higher than 100 MeV $27° < \theta < 153°$.

The number of events which passed this preliminary selection, was about 139000. Further selection was based on the kinematic fit of the events. Employing 4-momentum conservation it is possible with this procedure to build statistical tests for the different intermediate states in the observed event. For each event the following four hypotheses were tested:

(1) hypothesis $H_{2\gamma}$: two most energetic photons are due to the process $e^+e^- \to \gamma\gamma$. This hypothesis was used for the further suppression of spurious signals in the calorimeter,
(2) hypothesis $H_{3\gamma}$: three photons in the event are from the process (3),
(3) hypothesis $H_{\eta\gamma}$: three photons in the event are from the process (1),
(4) hypothesis $H_{\pi\gamma}$: three photons in the event are from the process (2).

One can notice that the hypotheses $H_{\eta\gamma}$ and $H_{\pi\gamma}$ are similar to the hypothesis $H_{3\gamma}$, but with the additional constraint on the invariant mass of the pair of photons. The performance of the kinematic fit procedure can be seen in Fig. 3, where the invariant mass spectra of all photon pairs are plotted, before and after the kinematic fit with the hypothesis $H_{3\gamma}$. A significant improvement of the resolution is clearly seen, especially for the $\eta$ meson mass.

For each of the above hypotheses a test statistics was build: $\xi_i = \text{Prob}(\chi^2_i)$, where $\chi^2_i$ is the $\chi^2$ value obtained in the kinematic fit under hypothesis $H_i$. For the correctly selected hypothesis the distribution of the corresponding statistics $\xi_i$ is close to uniform. Using these statistics the events which satisfy the $H_{3\gamma}$ hypothesis ($\xi_{3\gamma} > 0.003$) but do not satisfy the $H_{2\gamma}$ hypothesis ($\xi_{2\gamma} < 0.0005$) were selected. These events were divided further into 4 non-overlapping classes using the statistics $\xi_{\eta\gamma}$ and $\xi_{\pi\gamma}$:

(A.) a class containing mainly the events of the processes (1) and (3) ($\xi_{\eta\gamma} > \alpha$ and $\xi_{\pi\gamma} < \beta$),
(B.) a class containing mainly the events of the processes (2) and (3) ($\xi_{\pi\gamma} > \alpha$ and $\xi_{\eta\gamma} < \beta$),
(C.) a class containing the events of all three processes ($\xi_{\pi\gamma} > \beta$ and $\xi_{\eta\gamma} > \beta$),
(D.) a class containing mainly the events of the process (3) ($\xi_{\pi\gamma} < \beta$ and $\xi_{\eta\gamma} < \beta$),

where the parameters $\alpha = 0.05$ and $\beta = 0.0003$ define the size of the critical regions for the hypotheses $H_{\eta\gamma}$ and $H_{\pi\gamma}$. The number of events thus selected in each class is given in Table 1.

Tables 2–4 display the summary data for the above selection procedure. To reduce the size of these tables,

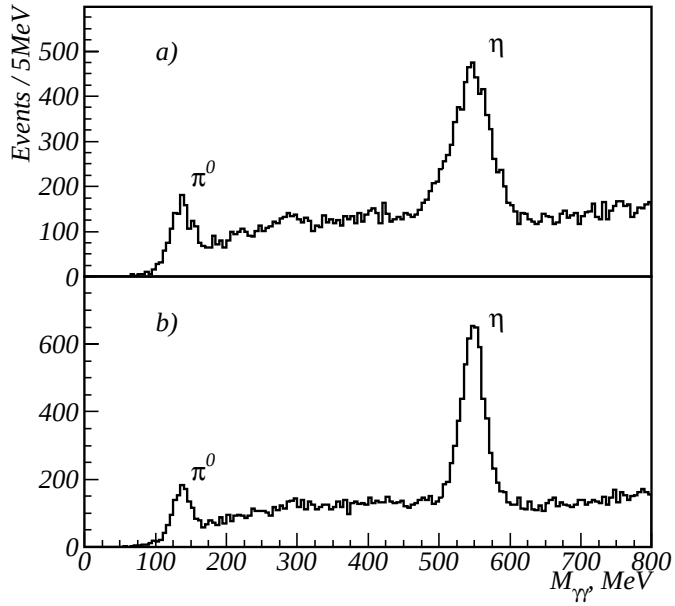


**Fig. 3a,b.** Comparison of spectra of the invariant masses of photon pairs in $3\gamma$ events before (plot **a**) and after (plot **b**) the $H_{3\gamma}$ kinematic fit. The spectra include three entries per event

**Table 1.** Number of events in each of the selection classes, and selection efficiencies in the $\phi$ resonance maximum

| Selection class | A | B | C | D |
|---|---|---|---|---|
| Total events | 20356 | 2224 | 2821 | 7376 |
| Process | | Efficiency, % | | |
| (1) | 44. | 0.02 | 2.4 | 0.3 |
| (2) | 0.1 | 14. | 11. | 0.3 |
| (3) | 1.2 | 0.31 | 0.31 | 4.1 |

the data points from different scans with close energies were merged together. Table 2 shows these combined data points, giving for each point the c.m. energy range and the integrated luminosity. Tables 3 and 4 show the data for the selection classes A and B, respectively. For each energy point these tables display the number of selected events, the selection efficiencies for the processes (1) or (2), the value of the factor $\beta_p$ (see (4) below) for each process, the expected number of events for the process (3), the resulting value of the cross section, and its error. We have to note here that the values of the cross sections in the tables are given for the reference only; our further analysis did not use them. Instead, the initial data were used.

## 4 Cross-section determination

For the determination of the parameters of the processes (1) and (2), the energy dependence of the observed number of events in each of four selection classes was approximated

**Table 2.** Experimental data points. Each entry contains the experimental point number, energy range for this point, and the integrated luminosity

| Point | Energy, MeV | | | Lumin., 1/nb | | |
|---|---|---|---|---|---|---|
| 1 | 985.13 | – | 986.04 | 195.1 | ± | 1.0 |
| 2 | 1004.51 | – | 1005.41 | 193.6 | ± | 1.0 |
| 3 | 1010.34 | – | 1011.19 | 248.8 | ± | 1.2 |
| 4 | 1015.62 | – | 1016.52 | 287.9 | ± | 1.2 |
| 5 | 1016.98 | – | 1017.34 | 239.0 | ± | 1.1 |
| 6 | 1017.94 | – | 1018.48 | 393.5 | ± | 1.4 |
| 7 | 1018.84 | – | 1019.43 | 1223.7 | ± | 2.4 |
| 8 | 1019.74 | – | 1020.39 | 489.4 | ± | 1.6 |
| 9 | 1020.72 | – | 1021.33 | 321.7 | ± | 1.4 |
| 10 | 1021.69 | – | 1021.95 | 184.6 | ± | 1.0 |
| 11 | 1022.14 | – | 1022.79 | 149.5 | ± | 0.9 |
| 12 | 1027.64 | – | 1028.59 | 198.7 | ± | 1.1 |
| 13 | 1033.38 | – | 1034.35 | 154.4 | ± | 0.9 |
| 14 | 1039.01 | – | 1039.30 | 23.9 | ± | 0.4 |
| Total: | | | | 4303.8 | | |

by the following dependence:

$$N_q^{\rm th}(E) = L(E) \times \sum_p \sigma_p(E)\beta_p(E)\varepsilon_{q,p}(E), \qquad (4)$$

where $N_q^{\rm th}(E)$ is the expected number of events in the selection class $q$, $L(E)$ is the integrated luminosity in the energy point, $\sigma_p(E)$ is the cross section of the process $p$, $\beta_p(E)$ is the factor taking into account radiative corrections [14] and the beam energy spread, and $\varepsilon_{q,p}(E)$ is the efficiency of the selection algorithm for process $p$ in the selection class $q$. Summation is performed over the three main processes (1), (2) and (3): the contribution from other processes, both resonant and non-resonant, estimated from the full simulation is negligible.

The integrated luminosity $L(E)$ was estimated from the number of events of two-photon annihilation at large angles ($27^\circ < \theta < 163^\circ$). The statistical uncertainty of the estimates is lower than 1% for most experimental points; systematic effects give an additional error of 2.5%.

For the description of the cross section of the processes $e^+e^- \to P\gamma$, where $P$ is a pseudoscalar meson, the following dependence was used:

$$\sigma(s) = \frac{4\pi\alpha^2 F(s)}{s^{3/2}} \left| B_P + {\rm i} \sum_{V=\rho,\omega,\phi} \frac{g_{VP\gamma}}{g_V} \frac{m_V^2 {\rm e}^{{\rm i}\varphi_V}}{D_V(s)} \right|^2, \qquad (5)$$

where $F(s) = \left[(s - m_P^2)/2s^{1/2}\right]^3$, and $D_V(s) = m_V^2 - s - {\rm i}s^{1/2}\Gamma_V(s)$. The amplitude $B_P$ describes the contribution from non-resonant intermediate states, its value being fixed by specific models as described below. The coupling constants $g_{VP\gamma}$ and $g_V$ are related to the decay widths of the vector meson $\Gamma(V \to P\gamma) = g_{VP\gamma}^2 F(m_V^2)/12\pi$ and $\Gamma(V \to e^+e^-) = 4\pi\alpha^2 m_V/g_V^2$. The contribution of the

**Table 3.** Summary table of the data for the selection class A. Each entry in the table contains the experimental point number, the number of selected events, the efficiency of the selection for the process (1), the factor $\beta$ from (4) for this process, the expected number of the events for the process (3), and the resulting cross section of the process $e^+e^- \to \eta\gamma$. The numbering of the energy points corresponds to Table 2

| Point | Events | Eff., % | $\beta$ | N QED | $\sigma_{e^+e^-\to\eta\gamma}$, nb |
|---|---|---|---|---|---|
| 1 | 98 | $39.7 \pm 0.8$ | 0.913 | 92.6 | $0.19 \pm 0.50$ |
| 2 | 98 | $43.4 \pm 0.3$ | 0.821 | 91.2 | $1.55 \pm 0.55$ |
| 3 | 226 | $43.7 \pm 0.3$ | 0.783 | 116.8 | $3.27 \pm 0.56$ |
| 4 | 893 | $43.9 \pm 0.2$ | 0.740 | 135.7 | $20.66 \pm 0.89$ |
| 5 | 1069 | $43.3 \pm 0.2$ | 0.729 | 110.8 | $32.43 \pm 1.18$ |
| 6 | 2351 | $43.5 \pm 0.2$ | 0.720 | 183.8 | $44.79 \pm 1.08$ |
| 7 | 9102 | $43.8 \pm 0.2$ | 0.729 | 577.1 | $55.59 \pm 0.70$ |
| 8 | 3369 | $43.4 \pm 0.2$ | 0.775 | 228.4 | $48.65 \pm 0.97$ |
| 9 | 1575 | $43.3 \pm 0.2$ | 0.854 | 149.9 | $30.55 \pm 0.91$ |
| 10 | 714 | $43.0 \pm 0.2$ | 0.930 | 85.4 | $21.72 \pm 0.99$ |
| 11 | 464 | $43.5 \pm 0.2$ | 1.000 | 70.1 | $15.47 \pm 0.91$ |
| 12 | 222 | $42.4 \pm 0.3$ | 1.659 | 92.0 | $2.37 \pm 0.32$ |
| 13 | 124 | $41.5 \pm 0.5$ | 2.636 | 71.5 | $0.79 \pm 0.21$ |
| 14 | 16 | $39.6 \pm 0.7$ | 3.978 | 10.9 | $0.35 \pm 0.35$ |
| Total: | 20356 | | | 2016.3 | |

excited states, such as $\rho'$ or $\rho''$, is expected to be small, and was not included in (5).

The energy dependence of the full widths of the vector mesons was determined from the sum of the widths of the principal decay modes, as in [6]. Particularly, the energy dependence of the $\rho$ meson width was taken as

$$\Gamma_\rho(s) = \Gamma_\rho(m_\rho^2)\frac{F(s)}{F(m_\rho^2)}\frac{m_\rho^2}{s}. \quad (6)$$

The cross section of the process $e^+e^- \to V \to P\gamma$ in the resonance maximum is given by

$$\sigma_{VP\gamma} = \frac{12\pi\Gamma_{V\to e^+e^-}\Gamma_{V\to P\gamma}}{m_V^2\Gamma_V^2}. \quad (7)$$

Using this relation and (5), the cross section of the process $e^+e^- \to P\gamma$ can be rewritten as

$$\sigma(s) = \frac{F(s)}{s^{3/2}}\left|\sqrt{4\pi\alpha^2}B_P + \mathrm{i}\sum_{V=\rho,\omega,\phi} A_V\right|^2, \quad (8)$$

$$A_V = \sqrt{\sigma_{VP\gamma}\frac{m_V^3}{F(m_V^2)}}\frac{m_V\Gamma_V e^{\mathrm{i}\varphi_V}}{D_V(s)}. \quad (9)$$

The cross sections of the processes $e^+e^- \to P\gamma \to \gamma\gamma\gamma$, which participate in fitting of the experimental data with (4), also include the probability of the decay $P \to \gamma\gamma$, $\sigma_p(s) = \sigma(s) \times \mathrm{Br}(P \to \gamma\gamma)$. The numbers obtained from the fitting of the experimental data with the dependence (4) are the values of the cross sections of the processes $e^+e^- \to \phi \to P\gamma \to \gamma\gamma\gamma$ in the resonance maximum

$$\sigma_{\phi P} \equiv \sigma_{\phi P\gamma} \times \mathrm{Br}(P \to \gamma\gamma); \quad (10)$$

the parameters of $\rho$ and $\omega$ mesons were fixed. As these values are obtained directly from the data, their errors include only the experimental uncertainties and the model dependence.

The selection efficiency for the processes (1) and (2) in each selection class was determined from the Monte Carlo simulation [15]. To reproduce the energy dependence of the efficiencies the simulation was performed in the whole energy region of the experiment, taking into account the radiative corrections. For the process (1) the energy dependence of the efficiency is rather weak and, to the desired precision, can be approximated by a parabolic curve. For the process (2) the dependence is stronger and more complex, determined by larger radiative corrections. For this process a simulation was performed with a more detailed scan of the energy region, with the further use of a linear approximation between the simulated energy points. The values for the efficiencies for each process in the resonance maximum are presented in Table 1.

The cross section of the process (3) was described using the formulae from [16], which do not take into account the radiative corrections. The efficiencies for this process were determined from the full simulation with the minimal energy of the emitted photons of 10 MeV and polar angles of $18^\circ < \theta < 162^\circ$. The efficiency obtained from Monte Carlo should be adjusted to take into account the influence of radiative corrections. For this, the factor $\beta_p$ (see (4)) for this process, which now includes both the radiative corrections and the efficiency adjustment, was determined from the fit of the experimental data of the selection class D. The value obtained in this way is $\beta = 0.96 \pm 0.01$. The resulting cross section fits well to the experimental data of the class D, thus allowing one to fix the level of the cross

**Table 4.** Summary table of the data for selection class B. Each entry in the table contains the experimental point number, the number of selected events, the efficiency of the selection for the process (2), the factor $\beta$ from (4) for this process, the expected number of the events for process (3), and the resulting cross section of the process $e^+e^- \to \pi^0\gamma$. The numbering of the energy points corresponds to Table 2

| Point | Events | Eff., % | $\beta$ | N QED | $\sigma_{e^+e^-\to\pi^0\gamma}$, nb |
|---|---|---|---|---|---|
| 1 | 39 | 6.7 ± 0.2 | 2.292 | 31.2 | 0.26 ± 0.28 |
| 2 | 37 | 8.5 ± 0.2 | 1.650 | 27.0 | 0.37 ± 0.30 |
| 3 | 70 | 10.0 ± 0.2 | 1.299 | 33.2 | 1.15 ± 0.32 |
| 4 | 135 | 12.6 ± 0.2 | 0.916 | 37.1 | 2.97 ± 0.40 |
| 5 | 103 | 13.3 ± 0.2 | 0.864 | 30.4 | 2.68 ± 0.64 |
| 6 | 276 | 13.7 ± 0.2 | 0.825 | 49.9 | 5.16 ± 0.42 |
| 7 | 920 | 14.1 ± 0.2 | 0.834 | 154.1 | 5.40 ± 0.25 |
| 8 | 346 | 13.3 ± 0.2 | 0.919 | 61.0 | 4.81 ± 0.35 |
| 9 | 133 | 12.7 ± 0.2 | 1.116 | 39.8 | 2.07 ± 0.29 |
| 10 | 68 | 11.7 ± 0.2 | 1.374 | 22.6 | 1.54 ± 0.33 |
| 11 | 48 | 11.3 ± 0.2 | 1.663 | 18.4 | 1.07 ± 0.29 |
| 12 | 29 | 7.0 ± 0.2 | 16.38 | 23.2 | 0.03 ± 0.03 |
| 13 | 19 | 4.9 ± 0.1 | 126.4 | 17.3 | 0.00 ± 0.01 |
| 14 | 1 | 4.1 ± 0.2 | 37.18 | 2.5 | -0.04 ± 0.05 |
| Total: | 2224 | | | 547.9 | |

section of the process (3) in all other selection classes. The uncertainty of the factor $\beta_p$ determined in this way does not influence the final results due to the relatively small contribution of this process to the selection classes A and B.

The fit of (4) to the experimental data was performed using the maximum likelihood method. The likelihood of an observation was described by a modified Poisson probability function, which takes into account the uncertainty of the mean value of the expected number of events.

To estimate the model dependence of the obtained results the fit of the experimental data was performed for the different theoretical models, described in the following sections.

### 4.1 Vector dominance model

In the vector dominance model (VDM) the cross section of the processes $e^+e^- \to P\gamma$ is determined only by the number of poles identified with the vector mesons [2,3], hence for VDM $B_P \equiv 0$. This is the most common model used for the description of the cross sections in practically all experiments with $e^+e^-$ colliding beams at low energies ($2E < 1$GeV).

The fitting of the observed number of events was performed simultaneously for the three selection classes, A, B, and C; the parameters determined from the fit were $\sigma_{\phi\eta}$ and $\sigma_{\phi\pi}$. For the masses and widths of all mesons their table values were used [17]. A consistent treatment of the model dependences requires the determination of all parameters in the same model. Following this approach the widths of the decays $\rho, \omega \to \eta\gamma$ and $\rho, \omega \to \pi^0\gamma$ were taken from the ND analysis [9], which was performed also using VDM.

In the case $B_P = 0$ there exists an uncertainty in the definition of the phases of vector mesons $\varphi_V$, thus the phase of $\rho$ meson was fixed at $\varphi_\rho = 0$. The value of the $\omega$ meson phase $\varphi_\omega$ was taken equal to $\varphi_\rho$, in accord with the quark model prediction. The value of the $\phi$ meson phase in the process (1) was set to $\varphi_\phi = 180°$. During the analysis of the data a strong dependence was observed of the obtained cross section $\sigma_{\phi\pi}$ on the phase value $\varphi_\phi$ in the process (2). An exact and independent determination of the phase $\varphi_\phi(\pi\gamma)$ from the same statistics is impossible. A fit was performed with a value $\varphi_\phi(\pi\gamma) = (158 \pm 11)°$, which was obtained by combination of the ND [9] and CMD-2 [18] measurements of this phase in the processes $e^+e^- \to \omega, \phi \to 3\pi$. The uncertainty of the phase was accounted for using the constrained fit technique.

As a result of the fit the following values of the cross section were obtained:

$$\sigma_{\phi\eta} = (22.16 \pm 0.20 \pm 0.59)\text{nb}, \quad (11)$$

$$\sigma_{\phi\pi} = (5.12 \pm 0.15^{+0.38}_{-0.35})\text{nb}. \quad (12)$$

In the quoted errors the first represent a statistical error, and the second the systematic one. The main contributors to the systematic errors are uncertainties in the integrated luminosity (2.5%), and in the efficiency evaluation: 1% for process (1), and 2% for process (2). For process (2) the uncertainty in the phase $\varphi_\phi$ was also included in the systematic error.

Using the table values of the decay probabilities [17],

$$\text{Br}(\eta \to \gamma\gamma) = (39.21 \pm 0.34)\%, \quad (13)$$

$$\text{Br}(\pi \to \gamma\gamma) = (98.798 \pm 0.0032)\%, \quad (14)$$

**Table 5.** Measured cross sections and branching ratios for the different models. Only statistical errors are quoted in this table

| $P$ | $\eta$ | $\pi^0$ |
|---|---|---|
| (I) VDM, $\varphi_\phi(\pi\gamma) = 158^\circ$ | | |
| $\sigma_{\phi P}$, nb | $22.16 \pm 0.20$ | $5.12 \pm 0.15$ |
| $\mathrm{Br}(\phi \to P\gamma)$ | $(1.338 \pm 0.012)\%$ | $(1.226 \pm 0.036) \times 10^{-3}$ |
| $\chi^2$/DOF | 212.4/211 | |
| (II) VDM, $\varphi_\phi(\pi\gamma) = 180^\circ$ | | |
| $\sigma_{\phi P}$, nb | $22.16 \pm 0.20$ | $5.82 \pm 0.16$ |
| $\mathrm{Br}(\phi \to P\gamma)$ | $(1.338 \pm 0.012)\%$ | $(1.396 \pm 0.036) \times 10^{-3}$ |
| $\chi^2$/DOF | 212.5/211 | |
| (III) Anomalous contribution | | |
| $\sigma_{\phi P}$, nb | $23.16 \pm 0.20$ | $5.39^{+1.12}_{-1.07}$ |
| $\mathrm{Br}(\phi \to P\gamma)$ | $(1.398 \pm 0.012)\%$ | $(1.29^{+0.27}_{-0.26}) \times 10^{-3}$ |
| $\varphi_\rho = \varphi_\omega$ | $(10 \pm 14)^\circ$ | $(52^{+11}_{-16})^\circ$ |
| $\varphi_\phi$ | $\varphi_\rho + 180^\circ$ | $(165^{+29}_{-39})^\circ$ |
| $\chi^2$/DOF | 210.7/208 | |
| (IV) Model-independent | | |
| $\sigma_{\phi P}$, nb | $21.7 \pm 1.3$ | $5.82^{+0.27}_{-0.82}$ |
| $\mathrm{Br}(\phi \to P\gamma)$ | $(1.31 \pm 0.08)\%$ | $(1.39^{+0.06}_{-0.20}) \times 10^{-3}$ |
| $\mathrm{Re}A$, nb$^{1/2}$ | $-0.74 \pm 0.18$ | $-0.78^{+0.08}_{-0.16}$ |
| $\mathrm{Im}A$, nb$^{1/2}$ | $0.18 \pm 0.81$ | $0.32^{+0.09}_{-0.32}$ |
| $\chi^2$/DOF | 212.0/207 | |

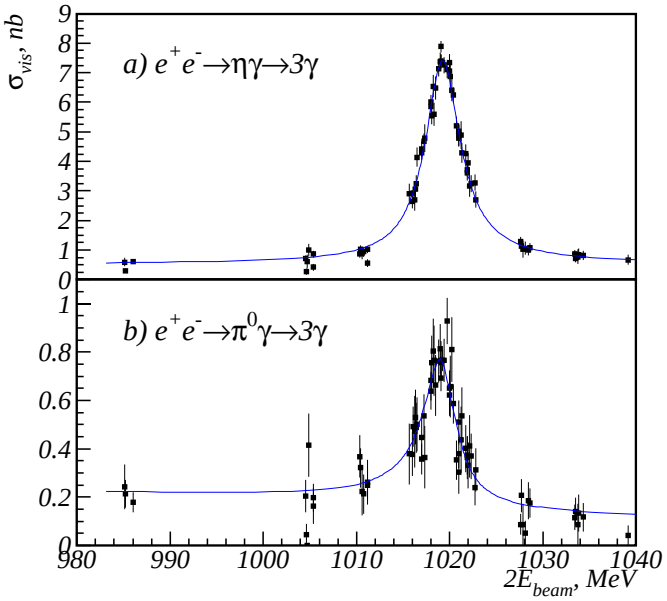


**Fig. 4a,b.** Visible cross section for the selection classes A (plot **a**) and B (plot **b**). The curves are the VDM fit

$$\mathrm{Br}(\phi \to e^+e^-) = (2.99 \pm 0.08) \times 10^{-4} \qquad (15)$$

from (11,12) the relative widths of the decays were obtained, which are given in part I of Table 5 together with the $\chi^2$ value obtained in the fit. Figure 4 represents the visible cross section, $\sigma_{\mathrm{vis}} = N/L$, in two selection classes for all experimental points together with the theoretical curves obtained from the fit.

For comparison, a fitting of the experimental data was also performed with the fixed value of the phase $\varphi_\phi(\pi\gamma) = 180^\circ$. The result, displayed in part II of Table 5, reveals a strong dependence of the decay width $\phi \to \pi^0\gamma$ on the exact value of this phase. The fit quality, measured by the value of $\chi^2$, in this case practically does not change.

### 4.2 Anomalous contribution

The next model discussed here is an extension of the VDM, and includes, in addition to the vector meson mediated diagrams, the contribution from the loop diagrams (anomalies). In this case $B_P$ in (5) determines the value of the anomalous contribution [5], and is related to the two-photon width of the pseudoscalar meson $\Gamma_{P\to\gamma\gamma}$:

$$B_P = -\sqrt{\frac{16}{3\alpha}\frac{\Gamma_{P\to\gamma\gamma}}{m_P^3}}. \qquad (16)$$

The value of this term is comparable in magnitude with the contribution of the $\rho$ and $\omega$ mesons in the resonance region. It is worth mentioning here that the phase of $B_P$ is fixed, thus allowing one to make the determination of the absolute value of phases $\varphi_V$ for all three vector mesons.

A fitting of the data was performed with (5) using the above expression for $B_P$. The free parameters in this fit were $\sigma_{\phi\eta}$, $\sigma_{\phi\pi}$, $\varphi_\rho(\eta\gamma)$, $\varphi_\rho(\pi\gamma)$ and $\varphi_\phi(\pi\gamma)$. All other phases were fixed according to the predictions of the quark model: $\varphi_\omega(\eta\gamma) = \varphi_\rho(\eta\gamma)$, $\varphi_\phi(\eta\gamma) = \varphi_\rho(\eta\gamma)+180^\circ$, $\varphi_\omega(\pi\gamma) = \varphi_\rho(\pi\gamma)$. For the reasons of consistence, mentioned already in the previous section, the widths of the decays $\rho, \omega \to \eta\gamma$ and $\rho, \omega \to \pi^0\gamma$ were taken from [5]. The set of parameters obtained as a result of the fit is displayed in part III of Table 5. Resulting cross sections differ from the values obtained for VDM; this fact is more noticeable for the $\phi \to \eta\gamma$ decay. For the $\phi \to \pi^0\gamma$ decay the obtained cross section is somewhat intermediate between the two VDM fits discussed above, but in this case the observed uncertainty in the cross section is larger than in the VDM case. This fact is determined by the total uncertainty in the $\phi$ meson phase and the strong correlation between these two values.

The values for the phases of vector mesons obtained for this model differ from those obtained in [5]. An additional fit was performed with the set of fixed phases obtained in [5]. A strong degradation of the quality of the fit was observed. The value of $\chi^2$ in this case is equal to 260 for 211 degrees of freedom, which indicates a rather low likelihood for the observed data in this variant. The discrepancy observed for the phases can, possibly, be attributed to the different parameterization of the $\rho$ shape used in [5], although we did not perform an exact analysis of its origin.

### 4.3 Model-independent check

An alternative approach to the parameterization of the cross section is based on the assumption about the near constant value of the non-resonant term of the amplitude, which includes pure non-resonant processes and also the tails of the $\rho$, $\omega$ mesons and possible higher states. This assumption should have a rather good precision in the energy region under study, which is quite narrow and remote from other resonances. Under this assumption the cross section of the process $e^+e^- \to P\gamma$ can be written as

$$\sigma_{e^+e^-\to P\gamma}(s) = \frac{F(s)}{s^{3/2}} \left|A_P - A_\phi\right|^2, \qquad (17)$$

where the energy-independent term $A_P$ determines the contribution of all intermediate mechanisms except $e^+e^- \to \phi \to P\gamma$, and $A_\phi$ is defined in (9). In this approach the parameters determined from the fit are $\sigma_{\phi\eta}$, $\sigma_{\phi\pi}$, and the complex amplitude $A_P$ for each of the processes under study.

The set of the parameters obtained from the fit is displayed in part IV of Table 5. As in the previous case, large uncertainties in the cross section values are observed, which come from the total uncertainty about the non-resonant amplitude $A_P$ and the strong correlation between $A_P$ and resulting cross section values. The $\chi^2$ value obtained for this fit is practically the same as for the above models, thus allowing one to draw a conclusion on the consistence of the assumption about the constant $A_p$ with the experimental data.

## 5 Discussion

As was already noted in the previous section, the results of the analysis of experimental data reveal a strong model dependence of the fitted values for cross sections and decay probabilities of the $\phi$ meson. Thus, it can be useful to compare other values obtained from these models. One particular thing in which the models differ is the description of the non-resonant amplitude.

For comparison, in each model we calculate the value of the non-resonant amplitude in the maximum of the $\phi$ meson. This amplitude includes both the true non-resonant amplitude (the $B_P$ term), and the tails of the $\rho$ and $\omega$ mesons. The phase of the resonant term was fixed at $\varphi_\phi = 180^\circ$ to bring the amplitude for each model to a form similar to (17). For VDM and the anomalous contribution the non-resonant amplitude is then represented as

$$A_P = \left[\mathrm{i}\sqrt{4\pi\alpha^2}B_P - \sum_{V=\rho,\omega} A_V\right] \mathrm{e}^{-\mathrm{i}\varphi_\phi}, \qquad (18)$$

where $B_P \equiv 0$ for VDM as before. For the model-independent approach the amplitude $A_P$ was used as obtained directly from the fit.

The amplitudes obtained are shown in Table 6. For the anomaly model the contribution from the $\rho$ and $\omega$ mesons and anomalies are displayed separately, together with their sum. For the model-independent approach the results displayed are the same as in Table 5. A comparison of the amplitudes from models (I–III) with the model-independent approach (IV) reveals no obvious discrepancies in the values of this non-resonant term. The values of $\chi^2$ (Table 5) also look favorable for all models. Thus, we conclude that the collected statistics is not sensitive enough to be able to discriminate between models or to exactly determine the model parameters. However, the difference between amplitudes observed for the different models (Table 6) at the level of one standard deviation may indicate that larger statistics can clarify the situation.

**Table 6.** Values of the non-resonant amplitude in the resonance maximum for different models. Errors given for the model-independent analysis (IV) are statistical only. Models (I) and (II) should have significantly smaller errors; for the model (III) the errors are the same as or smaller than those for the model-independent analysis (IV)

| $P\gamma$ | $\eta\gamma$ | $\pi^0\gamma$ |
|---|---|---|
| (I) VDM, $\varphi_\phi(\pi\gamma) = 158^\circ$ | | |
| $A$, nb$^{1/2}$ | $-0.99 + \mathrm{i}0.49$ | $-0.91 + \mathrm{i}0.03$ |
| (II) VDM, $\varphi_\phi(\pi\gamma) = 180^\circ$ | | |
| $A$, nb$^{1/2}$ | $-0.99 + \mathrm{i}0.49$ | $-0.82 + \mathrm{i}0.41$ |
| (III) Anomaly contribution | | |
| $A$, nb$^{1/2}(\rho+\omega)$ | $-0.70 + \mathrm{i}0.35$ | $-0.66 - \mathrm{i}0.56$ |
| $A$, nb$^{1/2}$(anom.) | $0.13 + \mathrm{i}0.72$ | $-0.19 + \mathrm{i}0.76$ |
| $A$, nb$^{1/2}$(total) | $-0.57 + \mathrm{i}1.07$ | $-0.85 + \mathrm{i}0.20$ |
| (IV) Model-independent | | |
| $A$, nb$^{1/2}$ | $-0.73 \pm 0.17$ $+\mathrm{i}(0.18 \pm 0.80)$ | $-0.78^{+0.08}_{-0.15}$ $+\mathrm{i}(0.32^{+0.09}_{-0.32})$ |

Despite the recent progress in the understanding of the anomalous contribution [5] there still remains a sort of ambiguity in its description, related also to the uncertainty in the parameterization of the shapes of the resonances. Due to this we consider our results obtained for the anomaly model as an indication of the necessity of further studies. Instead we prefer to conclude to the final result for the VDM model, because until now there is no strong evidence against VDM observed in the $e^+e^-$ data. This also allows one to compare these results directly with the results obtained earlier for the same model [9]. From (11) and (12) we obtain the following values for the triple products of the branching ratios:

$$\mathrm{Br}(\phi \to \eta\gamma) \times \mathrm{Br}(\phi \to e^+e^-) \times \mathrm{Br}(\eta \to \gamma\gamma) = (1.569 \pm 0.014 \pm 0.042) \times 10^{-6}, \quad (19)$$

$$\mathrm{Br}(\phi \to \pi^0\gamma) \times \mathrm{Br}(\phi \to e^+e^-) \times \mathrm{Br}(\pi^0 \to \gamma\gamma) = (3.62 \pm 0.10^{+0.27}_{-0.24}) \times 10^{-7}. \quad (20)$$

These values have the smallest relative systematic errors, as they are derived directly from the measured quantities.

Using the two-photon widths of $\eta$ and $\pi^0$ from (13) and (14) we obtain the values of the products

$$\mathrm{Br}(\phi \to \eta\gamma) \times \mathrm{Br}(\phi \to e^+e^-) = (4.00 \pm 0.04 \pm 0.11) \times 10^{-6}, \quad (21)$$

$$\mathrm{Br}(\phi \to \pi^0\gamma) \times \mathrm{Br}(\phi \to e^+e^-) = (3.67 \pm 0.10^{+0.27}_{-0.25}) \times 10^{-7}. \quad (22)$$

Eliminating the leptonic width of $\phi$ (see (15)) from these relations, we finally obtain the following values for the decay probabilities:

$$\mathrm{Br}(\phi \to \eta\gamma) = (1.338 \pm 0.012 \pm 0.052)\%, \quad (23)$$

$$\mathrm{Br}(\phi \to \pi^0\gamma) = (1.226 \pm 0.036^{+0.096}_{-0.089}) \times 10^{-3}, \quad (24)$$

where the systematic uncertainties include the errors quoted in (11) and (12) and uncertainties of the values $\mathrm{Br}(\phi \to e^+e^-)$ and $\mathrm{Br}(P \to \gamma\gamma)$ (13)–(15). The partial widths of the decays also include uncertainties from the $\Gamma_\phi$ determination, and are equal to

$$\Gamma(\phi \to \eta\gamma) = (58.9 \pm 0.5 \pm 2.4)\,\mathrm{keV}, \quad (25)$$

$$\Gamma(\phi \to \pi^0\gamma) = (5.40 \pm 0.16^{+0.43}_{-0.40})\,\mathrm{keV}. \quad (26)$$

In the determination of the partial widths of the decays $\phi \to \eta\gamma$ and $\phi \to \pi^0\gamma$ some of the systematic effects are common to both; hence in their ratio the errors caused by these effects cancel:

$$\frac{\Gamma(\phi \to \eta\gamma)}{\Gamma(\phi \to \pi^0\gamma)} = 10.9 \pm 0.3^{+0.7}_{-0.8}. \quad (27)$$

The uncertainty of the last result is still determined by the systematic effects, where the main contribution comes from the uncertainty in the $\phi$ meson phase in the process (2).

From the results of the work [11], which studied the cross section of the process $e^+e^- \to \phi \to \eta\gamma \to 3\pi^0\gamma$ using the same experimental data sets, we can also determine the ratio of the partial widths for the decays $\eta \to 3\pi^0$ and $\eta \to \gamma\gamma$,

$$\frac{\Gamma(\eta \to 3\pi^0)}{\Gamma(\eta \to \gamma\gamma)} = 0.796 \pm 0.016 \pm 0.016, \quad (28)$$

which is 1.1 standard deviation lower than the table value $0.821 \pm 0.007$ [17].

In Table 7 we give a comparison of our results for the decay probabilities with all previous measurements. Our measurements are close to the world average values (marked PDG in the table) and individual measurements. It is worth mentioning here that practically all cited analyses are based on some modification of a simple VDM approach. Hence all results of previous measurements are subjected to the model dependence discussed above, although it is significant only for the most precise measurements.

**Table 7.** Comparison of the observed decay probabilities with other recent measurements

| Experiment | Final state | $\mathrm{Br}(\phi \to \eta\gamma)$, % |
|---|---|---|
| This study | $3\gamma$ | $1.338 \pm 0.053$ |
| **PDG '98 [17]** | **avg.** | $1.26 \pm 0.06$ |
| SND '98 [11] | $7\gamma$ | $1.246 \pm 0.062$ |
| CMD-2 '95 [10] | $\pi^+\pi^-3\gamma$ | $1.18 \pm 0.11$ |
| ND '84 [9] | $3\gamma$ | $1.30 \pm 0.06$ |
| ND '84 [9] | $7\gamma$ | $1.4 \pm 0.2$ |
| OLYA '83 [19] | $3\gamma$ | $0.88 \pm 0.20$ |
| Andrews *et al.* '77 [20] | $3\gamma$ | $1.35 \pm 0.29$ |
| ORSAY '76 [21] | $3\gamma$ | $1.5 \pm 0.4$ |
| | | $\mathrm{Br}(\phi \to \pi^0\gamma)$, $10^{-3}$ |
| This study | $3\gamma$ | $1.23 \pm 0.10$ |
| ND '84 [9] | $3\gamma$ | $1.30 \pm 0.13$ |
| ORSAY '76 [21] | $3\gamma$ | $1.4 \pm 0.5$ |

## 6 Conclusion

The main results of these studies were presented in (11), (12), and (19-28). These results have a high statistical accuracy. Nevertheless, a precise determination of the decay parameters cannot be achieved without the essential reduction of the systematic errors and better understanding of the model dependence. In this respect the question is important of the detailed study of the non-resonant amplitude in the resonance region, both experimental and theoretical. In the experimental study improvement can be achieved with the precise study of the non-resonant region between $\omega$ and $\phi$, and above the $\phi$ meson. A further increase in the experimental statistics in the resonance region, especially at the slopes and tails of the resonance, will also help in understanding of the interference pattern of non-resonant and resonant terms. One more step in this direction could be the further analysis of the full statistics collected in the experiments SND and CMD-2, and the simultaneous analysis of different final states.

## References

1. L. Landsberg, Phys. Rep. **128**, 301 (1985)
2. P. O'Donnel, Rev. Mod. Phys. **53**, 673 (1981)
3. H. O'Connel et al., Prog. Part. Nucl. Phys. **39**, 201 (1997)
4. A. Bramon, A. Grau, G. Pancheri, Phys. Lett. B **344**, 240 (1995)
5. M. Benayoun et al., Z. Phys. C **72**, 221 (1996)
6. N. Achasov et al., Int. J. Mod. Phys. A **7**, 3187 (1992)
7. E. Anashkin et al., ICFA Instr. Bull. **5**, 18 (1988)
8. V. Aulchenko et al., in Proceedings of the Workshop on Physics and Detectors for DA$\Phi$NE (INFN, Frascati, 1991), p. 605
9. S. Dolinsky et al., Phys. Rep. **202**, 99 (1991)
10. R. Akhmetshin et al., Phys. Lett. B **364**, 199 (1995)
11. M. Achasov et al., JETP Lett. **68**, 573 (1998)
12. M. Achasov et al., Nucl. Instr. and Meth. A **411**, 337 (1998)

13. M. Bekishev, V. Ivanchenko, Nucl. Instr. and Meth. A **361**, 138 (1995)
14. E.A.Kurav, V.S.Fadin, Sov. J. Nucl. Phys. **41**, 466 (1985)
15. A. Bukin et al., in *MC91: Detector and Event Simulation in HEP* (NIKHEF-H, Amsterdam, 1991), pp. 79–85
16. B. Geshkenbein, M. Terentyev, J. Nucl. Phys. **8**, 550 (1968)
17. Particle Data Group, Eur. Phys. J. C **3**, (1998)
18. R. Akhmetshin et al., Phys. Lett. B **434**, 426 (1998)
19. L. Kurdadze et al., JETP Lett. **38**, 366 (1983)
20. D. Andrews et al., Phys. Rev. Lett. **38**, 198 (1977)
21. G. Cosme et al., Phys. Lett. B **63**, 352 (1976)